

# Preliminary study on the new wound monitoring technology using co-planar waveguide sensor: Modeling and simulation

Liang Zhang<sup>a</sup> and Zhenyu Ji<sup>b,\*</sup>

<sup>a</sup>*School of Basic Medical Science, Air Force Military Medical University, Xi'an, Shaanxi, China*

<sup>b</sup>*Faculty of Military Biomedical Engineering, Air Force Military Medical University, Xi'an, Shaanxi, China*

## Abstract.

**BACKGROUND:** Wound monitoring is very meaningful for the clinical research, diagnosis and treatment. But the existing wound monitoring technology is hard to meet the needs of modern medical care in terms of real-time, non-invasive and anti-interference.

**OBJECTIVE:** To solve this problem, this paper proposed a new kind of monitoring technology based on the co-planar waveguide transmission line theory and assessed the application value of this method as a wound monitoring technology.

**METHODS:** The simplified wound model included the skin, fat, muscle, tissue fluid and bandage and a new co-planar waveguide sensor were designed and established. All of the simulation was achieved in the electromagnetic special software. The data processing method was based on the transmission line theory.

**RESULTS:** Detailed analyses of the results from the simulation were conducted. The sensor has a good monitoring effect in the low frequency band. The monitoring results could be influenced by the thickness of the bandage outside the wound. The thickness of the bandage should not be larger than 10 mm. The effective monitoring area of the sensor is  $30 \times 20 \text{ mm}^2$ .

**CONCLUSIONS:** The proposed sensor based on the CPW transmission principle in this paper has good wound monitoring potential.

Keywords: CPW, electromagnetic field, impedance, monitoring technology, wound healing

## 1. Introduction

Wound healing is a very important and long process for patients. Wound monitoring can not only understand the injury in real time for effectively managing the wound [1], but also be helpful for clinical research and provides effective information for wound assessment and treatment plan [2]. As a result, wound monitoring is very meaningful for the wound healing process.

Modern wound monitoring should meet the environmental needs of mobile medicine. That means the monitoring technology should be efficient, accurate, convenient and non-invasive in order to adapt to various fields in reality such as engineering, military and so on. Existing wound monitoring technology is mainly based on the experience of clinical staff, using physical measurements such as wound area

---

\*Corresponding author: Zhenyu Ji, Faculty of Military Biomedical Engineering, Air Force Military Medical University, Xi'an, Shaanxi 710032, China. Tel.: +86 29 84776397; Fax: +86 29 84776397; E-mail: jizhenyu@fmmu.edu.cn.

Table 1  
The four-order Cole-Cole parameters of tissues for the model

Tissue	$\varepsilon_\infty$	$\Delta\varepsilon_1$	$\tau_1$ (ps)	$\alpha_1$	$\Delta\varepsilon_2$	$\tau_2$ (ns)	$\alpha_2$	$\Delta\varepsilon_3$	$\tau_3$ ( $\mu$ s)	$\alpha_3$	$\Delta\varepsilon_4$	$\tau_4$ (ms)	$\alpha_4$	$\sigma_s$
Skin	4.0	39.0	7.96	0.1	280	79.58	0	3e4	1.59	0.16	3e4	1.592	0.2	4e-3
Muscle	3.15	58.38	1.01	0.172	647.8	21.59	0.151	1245	4.17	0	37355	6.34	0	0.59
Fat	2.5	9.0	7.96	0.2	35	15.92	0.1	3.3e4	159.15	0.05	1e7	15.915	0.01	0.035
Tissue fluid	4.05	65.11	8.43	8e-3	595.6	11.06	6e-3	4889	1.94	0	17281	1.63	0	0.58
Tissue fluid (solidified)	3.75	58.18	1.09	3e-3	603.2	28	2e-3	2050	1.53	0	25530	1.01	0	0.03

and depth [3–5] or physiological measurements such as cell migration experiments [6] for evaluation. However, these methods are not convenient and real-time. The development of physics image technology represented by the optical coherence tomography (OCT) in the 1990s brought new breakthroughs to wound monitoring technology [7–9]. These technologies have good real-time performance and meet high-precision and non-invasive requirements. However, the OCT detection is susceptible to interference from external factors such as bandages, drugs, blood flow, etc., and its cost is relatively high because of the sensitive optical instrument.

Co-planar waveguide (CPW) is a relatively new type of electromagnetic transmission line device [10–12]. Compared with traditional waveguides, CPW that can achieve transmitting electromagnetic waves in a plane has the characteristics of conformal and miniaturization. As a result, the real-time, non-invasive monitoring can be realized based on the CPW transmission method. And due to the better penetration of electromagnetic fields, the ability to resist external interference of CPW should be stronger than that of OCT. Therefore, CPW has a high potential as a wound monitoring technology.

In this paper, the effect of a new transmission method based on CPW on wound status detection was studied through simulation based on the electromagnetic transmission line theory. According to the simulation results, the application value of this method as a wound monitoring technology was assessed.

## 2. Methods

### 2.1. Modeling of the wound of biological tissues

The simplified structure of hemorrhage injury was established to simulate the wound model of biological tissue, as shown in Fig. 1. The skin, fat, muscle, tissue fluid and bandage were contained in this structure. Blood was the main component of the tissue fluid.

As shown in Fig. 1, the main physical size parameters in the model include the thickness of each layer of tissue and bandage ( $h_{sk}$ ,  $h_{fa}$ ,  $h_{mu}$ ,  $h_{ba}$ ) and the radius and thickness of the tissue fluid ( $h_f$ ,  $R_f$ ). The dielectric properties ( $\varepsilon_r$ ,  $\sigma$ ) which are very important for the electromagnetic transmission calculation of each layer of tissues were derived through the actual measurement by our team [13] and Gebrial's team [14]. All measured data was finally imported into the model by fitted to the 4-order Cole-Cole equation as shown in Eq. (1) and Table 1. The dielectric properties of bandage were set to be 2.2 ( $\varepsilon_{r(ban)} = 2.2$ ), referred to existing literature on the dielectric properties of textile materials [15,16].

$$\hat{\varepsilon} = \varepsilon_\infty + \sum_{i=1}^4 \frac{\Delta\varepsilon_i}{1 + (j\omega\tau_i)^{(1-\alpha_i)}} + \frac{\sigma_s}{j\omega\varepsilon_0} \quad (1)$$

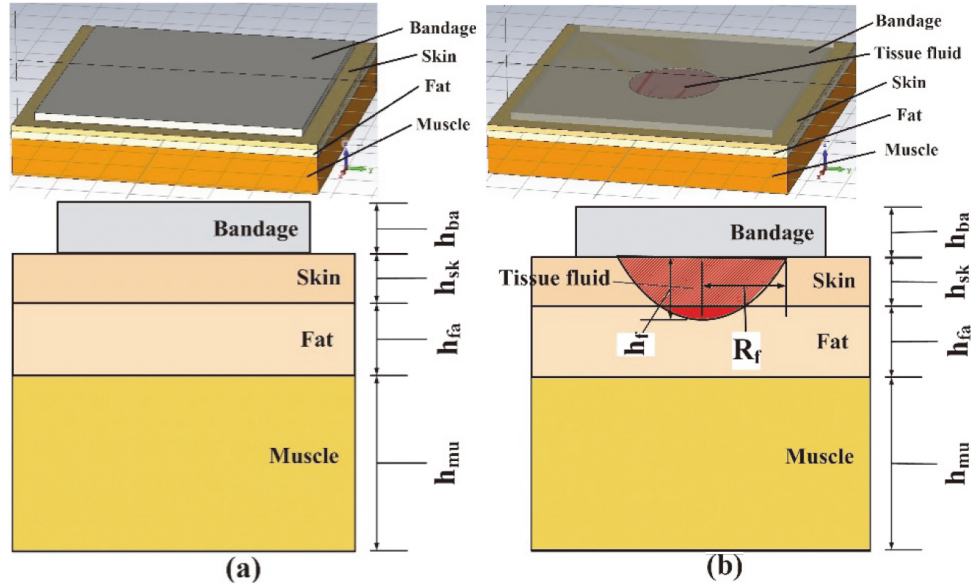


Fig. 1. The simplified structure of hemorrhage injury for simulation: (a) the normal tissue model, (b) the hemorrhage injury model.

## 2.2. Design of the sensor

The CPW structure was designed and applied to the simulation of this article, as shown in Fig. 2. The electromagnetic field would be distributed on the patch and be transmitted between port 1 and port 2 along the depth direction of the sensor. The main physical size parameters of this CPW structure were thickness and width ( $h_{pa}$ ,  $h_b$ ,  $w_{gap}$ ,  $w_{pa}$ ), which should be designed to make the characteristic impedance of sensor meet the requirements. The main component of patch is copper. A flexible circuit board called FPC ( $\epsilon_{r(FPC)} = 3.8$ ) that is mainly composed of polyimide as the main material would be used as the substrate medium in order to achieve the sensor conformal to biological tissues

## 2.3. Analysis of the sensor

As shown in Fig. 2, when the port 1 and port 2 were connected to the vector network analyzer at the same time, the transmission parameter matrix  $\mathbf{S}$  that describes the propagation characteristics of the electromagnetic field on the sensor can be measured. According to transmission line theory [17], the transmission scattering matrix  $\mathbf{S}$  can be converted into the transmission impedance matrix  $\mathbf{Z}$  of the sensor:

$$\mathbf{Z} = \begin{bmatrix} Z_{11} & Z_{12} \\ Z_{21} & Z_{22} \end{bmatrix} = Z_c(\mathbf{I} + \mathbf{S})(\mathbf{I} - \mathbf{S})^{-1} \quad (2)$$

In Eq. (2),  $Z_c$  is the characteristic impedance of the sensor which is decided to the physical size parameters of the sensor.  $\mathbf{I}$  is the identity matrix.  $Z_{ii}$  is the reflected impedance of port  $i$ , and  $Z_{ij}$  is the transmission impedance from port  $j$  to port  $i$ . When the two ports of the sensor are completely symmetrical, we can get  $Z_{11} = Z_{22}$  and  $Z_{12} = Z_{21}$ .

The transmission characteristics of the electromagnetic field on the sensor could be affected by changing in the media surrounding the sensor because of the changing of the dielectric properties ( $\epsilon_r$ ,  $\sigma$ ). Then the transmission scattering matrix  $\mathbf{S}$  and the transmission impedance matrix  $\mathbf{Z}$  would also be changed.

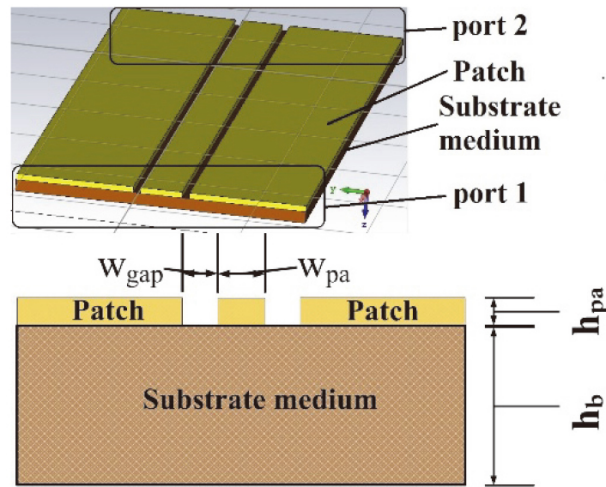


Fig. 2. The structure of the sensor for simulation.

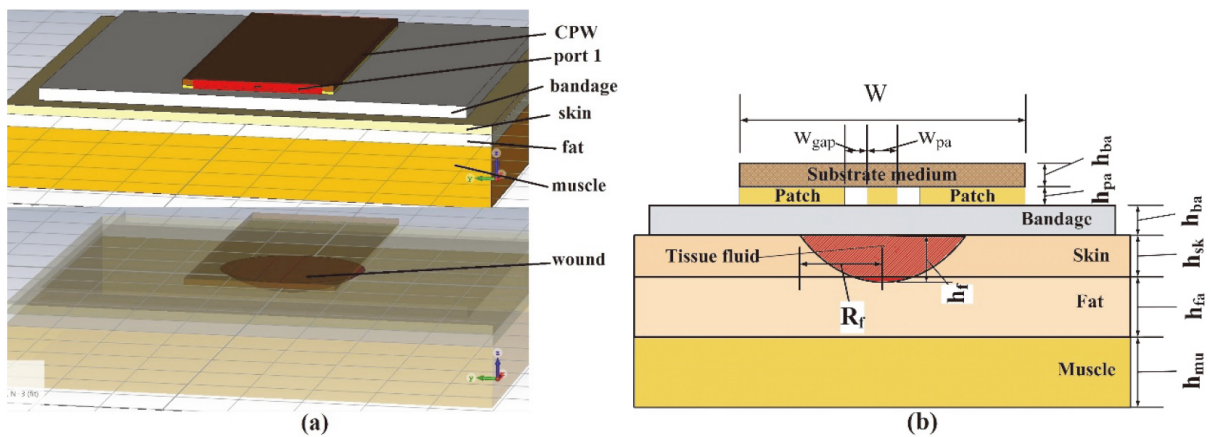


Fig. 3. The diagram of simulation settings: (a) simulation structure setting in CST (b) simulation structure size.

In other words, the parameters in the transmission impedance matrix  $\mathbf{Z}(\epsilon_r, \sigma)$  could be used to reflect the changes in the dielectric properties ( $\epsilon_r, \sigma$ ) of the media surrounding the sensor. While the dielectric properties ( $\epsilon_r, \sigma$ ) of biological tissues are closely related to their physiological properties [17]. As a result, the parameters in the transmission impedance matrix  $\mathbf{Z}(\epsilon_r, \sigma)$  could be used to detect the physiological state of biological tissues, when the sensor is attached to the surface of the tissue.

#### 2.4. Design of the simulation

Microwave Studio CST was used as the simulation software. Figure 3 shows the diagram of simulation settings. The sensor was attached to the surface of the bandage which wrapped around the wound. The wound was mainly composed of tissue fluid. The working frequency is set to 1–5 GHz. The structural parameters in the model are set as follows referring to the human physiological characteristics:  $w_{gap} = 0.63$  mm,  $w_{pa} = 3.54$  mm,  $h_{pa} = 0.5$  mm,  $h_b = 1.0$  mm,  $h_{ba} = 2$  mm,  $h_{sk} = 1.5$  mm,  $h_{fa} = 2.0$  mm,

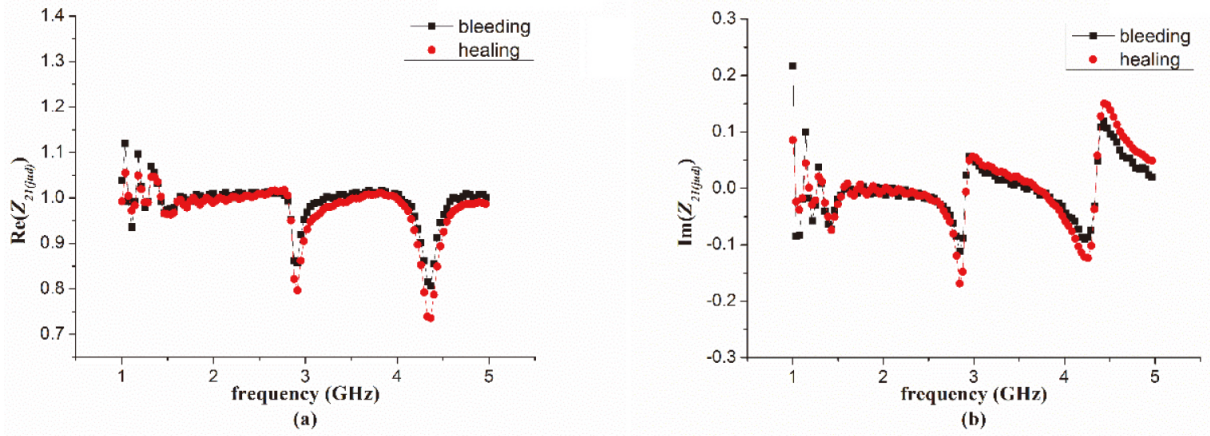


Fig. 4. The monitoring effect  $Z_{21(jud)}$  with  $W = 13.8$  mm: (a) the real part, (b) the imaginary part.

$h_{mu} = 10$  mm,  $h_f = 2$  mm,  $R_f = 10.19$  mm,  $W = 23.8$  mm. The characteristic impedance  $Z_c$  of sensor was  $50 \Omega$ , according to the physical size parameters.

In the simulation, the tested tissue was mainly composed of three states: normal state, bleeding state, and healing state. In the bleeding state and the healing state, the wound was mainly composed of tissue fluid and tissue fluid (solidified) whose dielectric characteristic parameters were shown in Table 1. On the other hand, several parameters such as  $W$  and  $h_{ba}$ , were taken as the variable quantities and compared for preliminary evaluating the potential capabilities of sensor for wound monitoring.

### 3. Results and discussion

#### 3.1. Data processing

According to Eq. (2), the transmission impedance matrix  $\mathbf{Z}$  was calculated by the transmission scattering matrix  $\mathbf{S}$  derived after simulation. the reflected impedance and transmission impedance also met the conditions:  $Z_{11} = Z_{22}$  and  $Z_{12} = Z_{21}$  due to the symmetry of sensor. As a result, only the reflected impedance  $Z_{11}$  and transmission impedance  $Z_{21}$  from port 1 were considered here, both of which were complex numbers. The new normalization complex parameter  $Z_{ij(jud)}$  was introduced to quantify the wound detection capability of the sensor.  $Z_{ij(jud)}$  could be defined by the calculated impedance  $Z_{ij}$  of tested tissue with three states:

$$Z_{ij(jud)} = \frac{Z_{ij(wound)}}{Z_{ij(normal)}} \quad (3)$$

According to Eq. (3), the real part of normalization complex parameter  $Z_{ij(jud)}$  should deviate from the value 1, and the imaginary part should deviate from the value 0, when there was a wound on the tissue. The deviation of  $Z_{ij(jud)}$  was related to the dielectric properties of the wound, which could be used to assess wound status.

#### 3.2. Study of the monitoring effect $Z_{21(jud)}$ with the different widths $W$ of sensor

The size parameters of the sensor designed by different team could be different. But most of the size parameters would not differ too much in order to make the characteristic impedance of the sensor equal

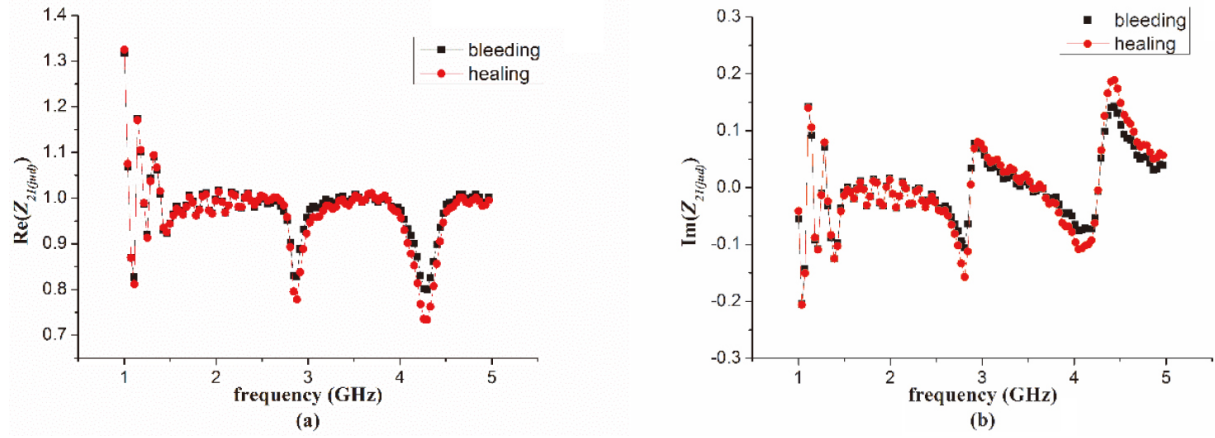


Fig. 5. The monitoring effect  $Z_{21(jud)}$  with  $W = 23.8$  mm: (a) the real part, (b) the imaginary part.

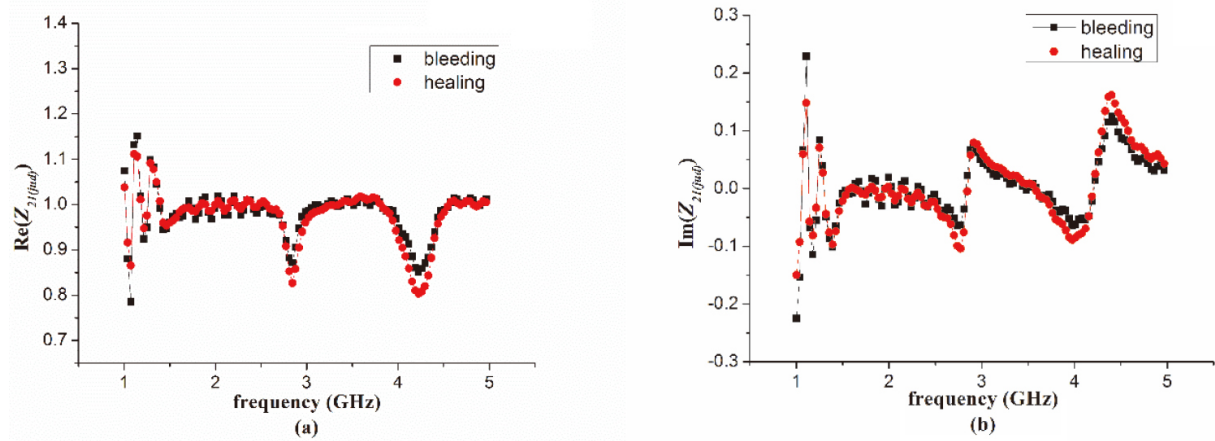


Fig. 6. The monitoring effect  $Z_{21(jud)}$  with  $W = 33.8$  mm: (a) the real part, (b) the imaginary part.

to  $50 \Omega$  under the premise of considering the manufacturing process, in addition to the width  $W$  of the sensor. Figures 4–6 show the monitoring effect  $Z_{21(jud)}$  with the different widths  $W$  of sensor after simulation.

As shown in Figs 4–6, the real part and the imaginary part of  $Z_{ij(jud)}$  were farther from the value 1 and in the low frequency band and at the resonance frequency points. There was also a significant difference in the value of  $\text{Re}(Z_{ij(jud)})$  and  $\text{Im}(Z_{ij(jud)})$  in the two states of bleeding and healing. That means the sensor had a better wound monitoring effect at low frequency bands. The reason may be that the electromagnetic field penetration ability was relatively high which made the anti-interference ability of the sensor stronger, when the frequency was low. While there were also several resonance points at the high frequency band, where the sensor has also achieved better monitoring results. In the other frequency bands, the monitoring results of the sensor were not good.

Comparing with Figs 4–6, it was found that the change of  $W$  had little effect on the overall monitoring effect of the sensor. Therefore, the design size has little effect on the ability of the sensor to monitor wounds. That implies the general applicability of the sensor is good.

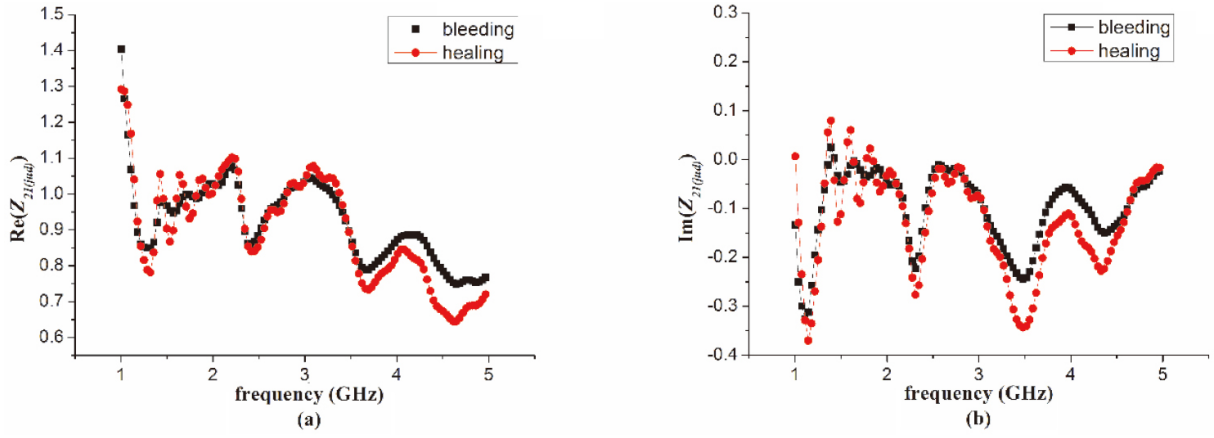


Fig. 7. The monitoring effect  $Z_{21(jud)}$  with  $h_{ba} = 0.5$  mm ( $W = 23.8$  mm): (a) the real part, (b) the imaginary part.

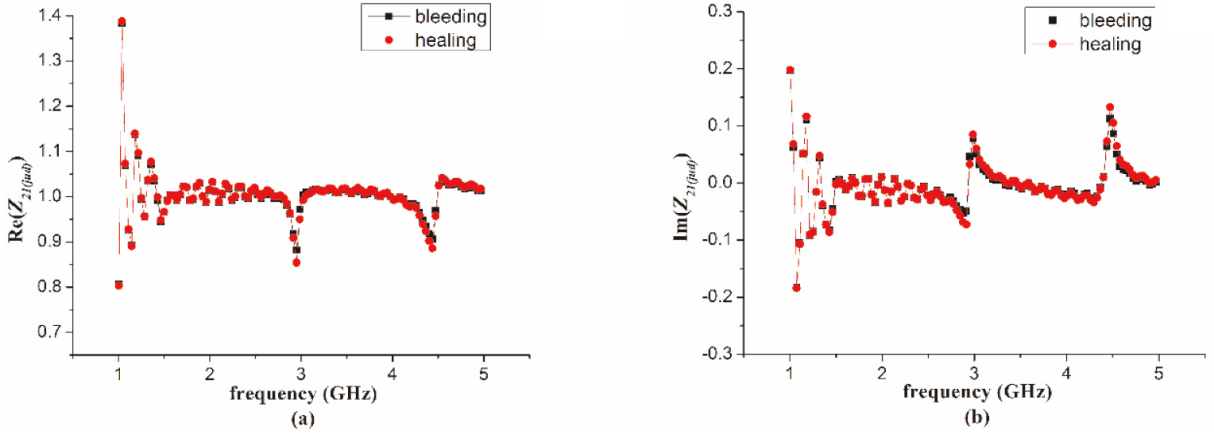


Fig. 8. The monitoring effect  $Z_{21(jud)}$  with  $h_{ba} = 4$  mm ( $W = 23.8$  mm): (a) the real part, (b) the imaginary part.

### 3.3. Study of the monitoring effect $Z_{21(jud)}$ with the different thickness $h_{ba}$ of bandage

Figures 7 and 8 show the monitoring effect  $Z_{21(jud)}$  with the different thickness  $h_{ba}$  of the bandage outside of the wound that could affect the sensor monitoring.

As shown in Fig. 7, the best monitoring results of the sensor were achieved in the working frequency range, when the thickness of the bandage was thin ( $h_{ba} = 0.5$  mm). It was found that the numerical distinction of  $\text{Re}(Z_{ij(jud)})$  and  $\text{Im}(Z_{ij(jud)})$  in the two states of bleeding and healing was very low in Fig. 8. That implies the sensor could monitor the wound status through the bandage, but the monitoring effect would be influenced by the thickness of the bandage. The thickness of the bandage should not be too large in the actual monitoring process.

### 3.4. Study of the monitoring effect determined by $Z_{11(jud)}$

According to the transmission line theory [17],  $Z_{21}$  describes the characteristics of electromagnetic field transmission from port 1 of the sensor to port 2. While  $Z_{11}$  describes the characteristics of electromagnetic

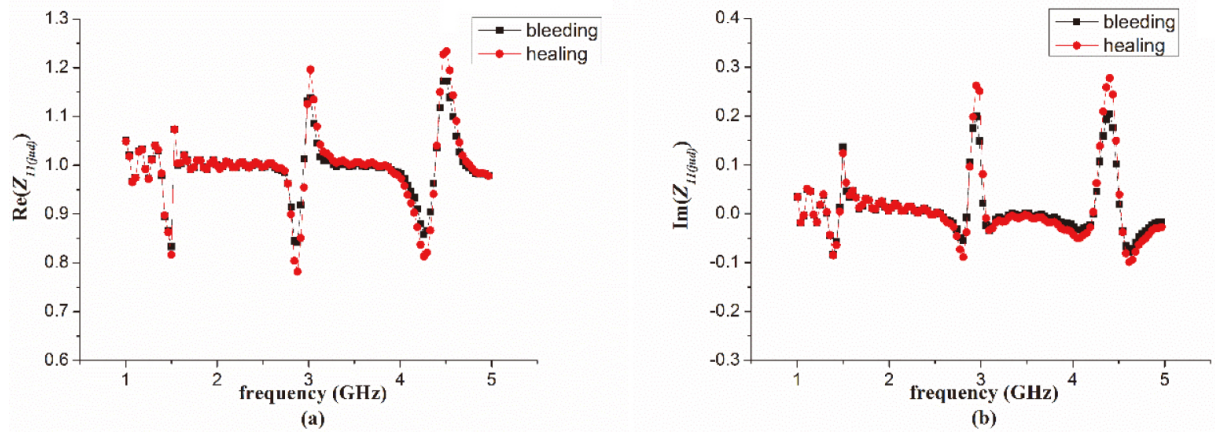


Fig. 9. The monitoring effect  $Z_{11(jud)}$  with  $h_{ba} = 2$  mm ( $W = 23.8$  mm): (a) the real part, (b) the imaginary part.

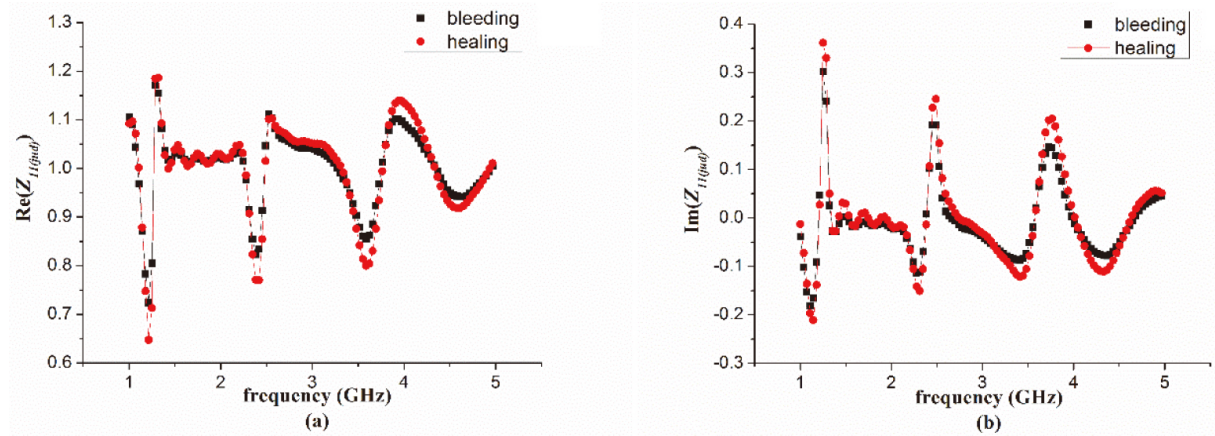


Fig. 10. The monitoring effect  $Z_{11(jud)}$  with  $h_{ba} = 0.5$  mm ( $W = 23.8$  mm): (a) the real part, (b) the imaginary part.

field being excited from the sensor port 1 and returning to port 1 after reflection. Both  $Z_{11}$  and  $Z_{21}$  should contain information about the dielectric properties of tissues surrounding the sensor which was carried by the electromagnetic field during transmission. As a result, the results of the assessment of the wound monitoring ability of the sensor with  $Z_{11}$  should be equivalent to results with  $Z_{21}$ . Figures 9 and 10 show the monitoring effect  $Z_{11(jud)}$  with the different parameters.

As shown in Figs 9 and 10, there were also several resonance points at the high frequency band, where the sensor has also achieved better monitoring results. The resonance frequency points were consistent with the resonance frequency points in the monitoring results with  $Z_{21(jud)}$  under the corresponding conditions, as shown in Figs 5 and 7. The real part and the imaginary part of  $Z_{11(jud)}$  were also farther from the value 1 and in the low frequency band and at the resonance frequency points. The significant difference in the value of  $\text{Re}(Z_{11(jud)})$  and  $\text{Im}(Z_{11(jud)})$  in the two states of bleeding and healing was also derived near the resonance frequency points in Figs 9 and 10. This conclusion was consistent with the previous results of  $Z_{21}$  which means the parameter  $Z_{11(jud)}$  could also be used for wound monitoring

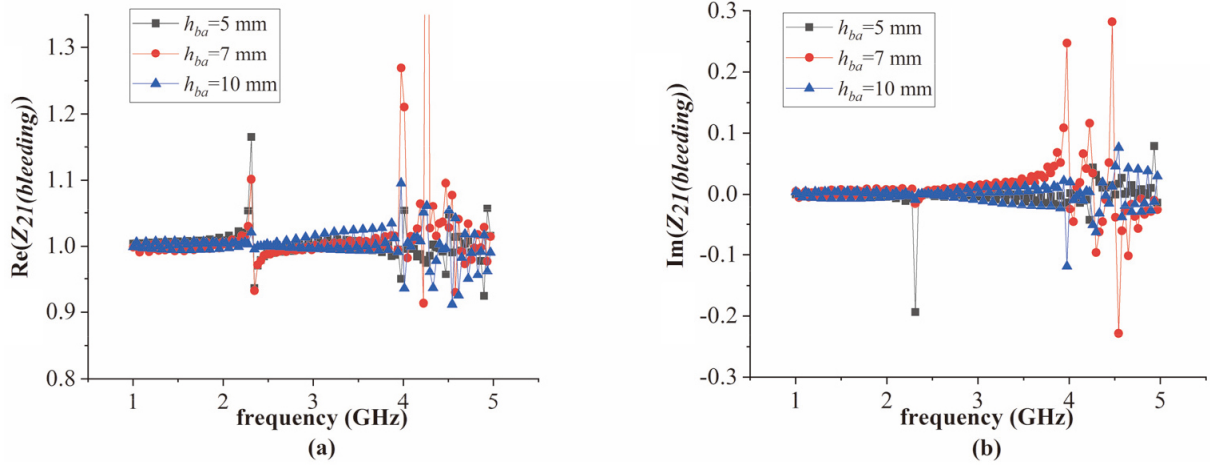


Fig. 11. The monitoring effect  $Z_{21}(\text{bleeding})$  with different  $h_{ba}$  ( $W = 13.8$  mm): (a) the real part, (b) the imaginary part.

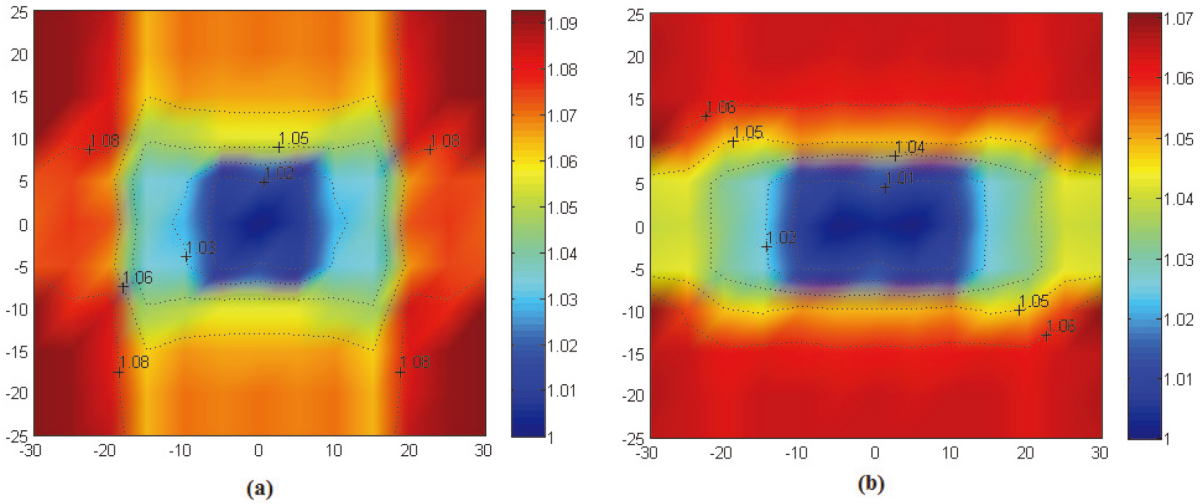


Fig. 12. The imaging results of real part of  $Z_{21}(\text{jud})$  scanned by the sensor at 2.95 GHz: (a) the bleeding state, (b) the healing state.

### 3.5. Study on the range of the sensor monitoring area

In order to determine the effective monitoring area range of the sensor proposed in this paper, the monitoring effect  $Z_{21}(\text{jud})$  with several other thickness  $h_{ba}$  of bandage and the imaging results scanned by the sensor within the wound area were studied and obtained in this section. Figure 11 shows the monitoring effect  $Z_{21}(\text{bleeding})$  for the with other different thickness  $h_{ba}$  of bandage when the widths  $W$  of sensor was determined ( $W = 13.8$  mm).

As shown in Fig. 11, The real part and the imaginary part of  $Z_{21}(\text{bleeding})$  began to approximate the value 1 and in the entire working frequency band, when the thickness  $h_{ba}$  of bandage was 10 mm. This shows that the monitoring effect of the sensor would be very insignificant when the thickness  $h_{ba}$  of bandage is greater than 10 mm.

Sometimes the sensor may not be able to place on the center of the wound accurately. In order to

determine the monitoring area size of the sensor, we changed the position of the sensor on the bandage plane in the simulation model in Fig. 3b and studied the monitoring effect. The thickness  $h_{ba}$  of bandage was set to be 2 mm. The widths  $W$  of sensor was set to be 13.8 mm. To improve the simulation efficiency, the position of the sensor was changed in two orthogonal directions on the bandage plane. The moving step was set to be 5 mm. The moving range of the sensor was set to be as  $60 \times 50 \text{ mm}^2$ . Figures 12 shows the imaging results scanned by the sensor at 2.95 GHz, which is one of the resonance frequency point shown in Fig. 4a.

In Fig. 12, the imaging results show the obvious numerical difference in the area of  $30 \times 20 \text{ mm}^2$ . This indicated that the sensor could effectively monitor the wound status within this range. On the other hand, the wound in Fig. 12 shows a rectangular area instead of the circular area in Fig. 3. That is because the position of the sensor on the bandage plane in the simulation model in Fig. 3b was changed along the rectangular area. The step size was relatively large. As well as, the resolution of the imaging was low.

#### 4. Conclusion

According to the simulation results, the proposed sensor based on the CPW transmission principle in this paper has good wound monitoring potential. The sensor has a good monitoring effect due to the electromagnetic penetration in the low frequency band where is near the 1 GHz frequency point. The monitoring results would be influenced by the thickness of the bandage outside the wound. As a result, the thickness of the bandage should not be larger than 10 mm. The effective monitoring area of the sensor is  $30 \times 20 \text{ mm}^2$ .

The results of the assessment of the wound monitoring ability of the sensor with  $Z_{11}$  should be equivalent to results with  $Z_{21}$ . However, it is worth to study a way to combine these two parameters to assess the effect of sensor monitoring for the better results. On the other hand, both of the reflected impedance  $Z_{11}$  and transmission impedance  $Z_{21}$  contain the information about the dielectric properties of the measured tissues. A new data analysis method for wound monitoring could be provided by establishing the relationship between impedance and dielectric characteristic parameters ( $Z_{11}, Z_{21} \sim \epsilon_r, \sigma$ ). All of these should be studied in future research process.

#### Acknowledgments

This research was supported by NSFC (No. 81671846), the National Key R&D Program (2019YFC0119103), and FSPTF (No. 2019-JCJQ-JJ-090).

#### Conflict of interest

None to report.

#### References

- [1] Gogia SB. A novel and accurate technique of photographic wound measurement. Indian Journal of Plastic Surgery. 2019; 45(2): 425-429.
- [2] Wang SC, Au Y, Ramirez JL, et al. The promise of smartphone applications in the remote monitoring of postsurgical

- wounds: a literature review. *Advances in Skin & Wound Care*. 2020; 33(9): 489-496.
- [3] Sattar H, Bajwa IS, Amin RU, et al. An IoT-based intelligent wound monitoring system. *IEEE Access*. 2019; 7: 144500-144515.
- [4] Smaropoulos E, Cremers NA. Medical grade honey for the treatment of paediatric abdominal wounds: a case series. *Journal of Wound Care*. 2020; 29(2): 94-99.
- [5] Pena G, Kuang B, Szpak Z, et al. Evaluation of a novel three-dimensional wound measurement device for assessment of diabetic foot ulcers. *Advances in Wound Care*. 2020; 9(11): 623-631.
- [6] Augustine R, Hasan A, Patan NK, et al. Titanium nanorods loaded PCL meshes with enhanced blood vessel formation and cell migration for wound dressing applications. *Macromolecular Bioscience*. 2019; 19(7): e1900058-e1900072.
- [7] Glinos GD, Verne SH, Aldahan AS, et al. Optical coherence tomography for assessment of epithelialization in a human *ex vivo* wound model. 2017; 25(6): 1017-1026.
- [8] Deegan A, Wang W, Men S, et al. Optical coherence tomography angiography monitors human cutaneous wound healing over time. *Quantitative Imaging in Medicine and Surgery*. 2018; 8(2): 135-150.
- [9] Chiu WK, Vien BS, Russ M, et al. Towards a non-invasive technique for healing assessment of internally fixated femur. *Sensors*. 2019; 19(4): 857-870.
- [10] Arshad S, Tahir FA, Rashid A, et al. Coplanar-waveguide fed circularly polarized antenna for wireless WLAN/LTE applications. *Electromagnetics*. 2020; 40(5): 354-363.
- [11] Nanda M, Kalavagunta Y, Rajareddy AV. A quad-band sierpenski based fractal antenna fed by coplanar waveguide. *Microwave & Optical Technology Letters*. 2020; 62(2): 893-898.
- [12] Mahajan RC, Parashar V, Vyas V, et al. Design and implementation of defected ground surface with modified co-planar waveguide transmission line. *SN Applied Sciences*. 2019; 1(3): 251-262.
- [13] Zhang L, Pang Y, Ding L, et al. The cole-cole model of porcine activity tissues in radio frequency. 10th International Congress on Image and Signal Processing & BioMedical Engineering and Informatics. 2017; 1-4.
- [14] Gabriel S, Lau RW, Gabriel C. The dielectric properties of biological tissues: III. Parametric models for the dielectric spectrum of tissues. *Physics in Medicine and Biology*. 1996; 41(11): 2271--2293.
- [15] Sara A, Elham M, Karoliina K, et al. Design and optimization of mm-size implantable and wearable on-body antennas for biomedical systems. The 8th European Conference on Antennas and Propagation. 2014; 1-5.
- [16] Jose A, Kappan SJ. High gain coplanar feed ultra-wide band wearable antenna using artificial magnetic conductors. 5th International Conference on Advances in Computing and Communications. 2015; 1-4.
- [17] Harrington RF editors. *Time-harmonic electromagnetic fields*. 2ed. New York: McGraw-Hill; 1961. pp. 398-402.